Prompt efficiency of energy harvesting by magnetic coupling of an improved bi-stable system*

Hai-Tao Li(李海涛) and Wei-Yang Qin(秦卫阳)†

Department of Engineering Mechanics, Northwestern Polytechnical University, Xi'an 710072, *China*

(Received 25 April 2016; revised manuscript received 18 July 2016; published online 30 September 2016)

In order to improve the transform efficiency of bi-stable energy harvester (BEH), this paper proposes an advanced bi-stable energy harvester (ABEH), which is composed of two bi-stable beams coupling through their magnets. Theoretical analyzes and simulations for the ABEH are carried out. First, the mathematical model is established and its dynamical equations are derived. The formulas of magnetic force in two directions are given. The potential energy barrier of ABEH is reduced and the snap-through is liable to occur between potential wells. To demonstrate the ABEH's advantage in harvesting energy, comparisons between the ABEH and the BEH are carried out for both harmonic and stochastic excitations. Our results reveal that the ABEH's inter-well response can be elicited by a low-frequency excitation and the harvester can attain frequent jumping between potential wells at fairly weak random excitations. Thus, it can generate a higher output power. The present findings prove that the ABEH is preferable in harvesting energy and can be optimally designed such that it attains the best harvesting performance.

Keywords: vibration energy harvesting, bi-stability, nonlinear dynamics, coherence resonance

PACS: 05.40.–a, 77.65.–j **DOI:** 10.1088/1674-1056/25/11/110503

1. Introduction

The rapid advancement in low-power electrical systems such as sensors in recent decades has led to the great increase of the requirement for the technology of self-power. Harvesting energy from an ambient vibration has attracted considerable interest because it could provide electrical energy for sensors and other micro-electrical devices in a portable and sustainable way.

Among different energy transduction mechanisms, piezoelectric energy harvesters show superior conversion efficiency and can be manufactured in both micro-scale and macro-scale. Initially, studies of the vibration-based energy harvester adopted the linear resonance theory. However, the vibrations existing in most environments are made up of a number of frequencies instead of a single frequency, the linear energy harvester becomes incapable of efficiently harvesting in this environment.[1–3]

To overcome the defect of the narrow bandwidth of linear harvesters, various approaches have been proposed to broaden the bandwidth, e.g., oscillator arrays and active frequency tuning method.[4,5] Another significant improvement in broadening the bandwidth is achieved by introducing nonlinearity, such as mono-stability,[6–9] bi-stability,[10–14] tri-stability,[15–17] and impact,[18] into the design of energy harvesters. Stanton *et al.*[19] studied the piezoelectric bi-stable harvester and provided the mathematical expression of magnetic repulsion force. Erturk *et al.*[20] extended the application of the bistable mechanism of Moon[21] to improve the energy harvesting performance and reported that an order of power output over the linear system without magnets. Wang *et al.*[22] proposed an elastic magnifier to magnify the base vibration displacement to enhance the output characteristic of the bistable oscillator. Zhou *et al.*[23] investigated the piezomagnetic harvester for enhancing broadband frequency response by altering the angle of two external magnets. Fan *et al.*[24] improved the performance of piezoelectric energy harvester by using the magnetic coupling of two cantilever beams.

Since the ambient vibration source generally includes many frequency components, even a continuous spectrum in the frequency domain, a few researchers have investigated energy harvesting under stochastic excitation. Litak *et al.*[25] used numerical methods to investigate the performance of a bistable energy harvester under random excitation and the results showed that the system can attain stochastic resonance. Li *et al.*[26] undertook numerical and experimental investigations on the stochastic resonance of a tri-stable harvester, and the results demonstrated that it has a better performance compared with the bistable energy harvester under stochastic excitations.

For a bi-stable energy harvester system, broadband excitations may induce its response to take a nearly regular jump between two stable positions (coherence resonance), for which the signal to noise ratio will yield a peak.[27,29] Cao *et al.*[30] found that the threshold of inter-well oscillation of a bi-stable configuration was dependent on the depth of potential wells. Hosseninloo *et al.*[31] studied an energy harvester with an

*Project supported by the National Natural Science Foundation of China (Grant No. 11172234) and the Scholarship from China Scholarship Council (Grant No. 201506290092).

†Corresponding author. E-mail: qinweiyang67@gmail.com

© 2016 Chinese Physical Society and IOP Publishing Ltd

adaptive bistable potential, which can be adjusted by an adaptive controller. However, this strategy needs to consider the balance between the energy consumed by the controller and that generated by piezoelectric patches.

This paper presents a new idea to reduce the potential barrier in BEH and elicit the occurrence of snap-through under low-intensity excitation. The rest of this paper is organized as follows. In Section 2, an electromechanical model of the advanced bi-stable energy harvester (ABEH) is established and analytically studied by using the extended Hamilton's principle. In Section 3, numerical simulations are carried out to analyze the dynamical response under deterministic and stochastic excitations. The results validate that the ABEH can work more efficiently than its conventional bi-stable counterpart. The summary is finally concluded in Section 4.

2. Analysis of the model

Figure 1 illustrates the model of traditional bistable energy harvester (BEH) and the proposed advanced bi-stable energy harvester (ABEH) with two movable magnets. As shown in Fig. 1(b), the ABEH includes two elastic beams, a cantilever beam, and a clamped beam. The cantilever beam has a magnet A at the tip, while the clamped beam has a magnet B at the middle. The aim of introducing the clamped beam is to turn the BEH's fixed magnet into a movable magnet.

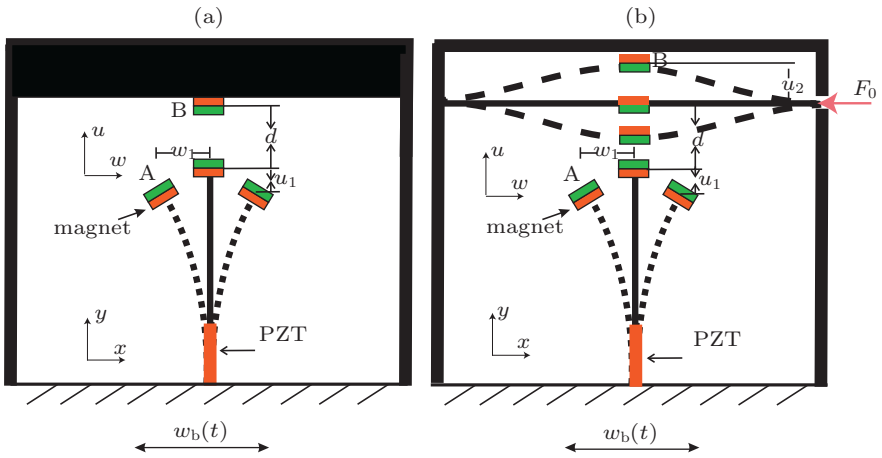


Fig. 1. (color online) (a) Traditional bi-stable energy harvester; (b) advanced bi-stable energy harvester.

In the following analysis, subscripts 1 and 2 refer to the cantilever beam and the clamped beam, respectively, E_{k1} and E_{k2} denote the kinetic energies of the cantilever beam and the clamped beam, respectively. Then, the total kinetic energy can be given by

$$\begin{aligned} E_k &= E_{k1}+E_{k2} \\ &= \frac{1}{2}\int_0^{L_1} m_1\left((\dot{w}_1+\dot{w}_b)^2+\dot{u}_1^2\right)\mathrm{d}y+\frac{1}{2}\int_0^{L_2} m_2(\dot{u}_2)^2\mathrm{d}x \\ &\quad +\frac{1}{2}M_1\left((\dot{w}_1(L_1,t)+\dot{w}_b)^2+\dot{u}_1(L_1,t)^2\right) \\ &\quad +\frac{1}{2}M_2\dot{u}_2(L_2/2,t)^2, \end{aligned} \tag{1}$$

where L_1 and L_2 are the lengths of the piezoelectric beam and the clamped beam, respectively, w and u denote the displacements of the beams in x and y directions, respectively, m_1 and m_2 are the masses per unit length of the cantilever beam and the clamped beam, respectively, and they can be calculated by

$$\begin{aligned} m_1 &= b\delta_1\rho_1+b\delta_p\rho_p\left[\mathrm{H}\left(y-\frac{L_1-L_p}{2}\right)-\mathrm{H}\left(y-\frac{L_1+L_p}{2}\right)\right], \\ m_2 &= \rho_2 b\delta_2, \end{aligned} \tag{2}$$

where δ_1, δ_2, and δ_p represent the thicknesses of the beams and the piezoelectric layer, respectively; L_p is the length of the piezoelectric material; ρ_1, ρ_2, and ρ_p represent the densities of the beam material and the piezoelectric material respectively; b represents the widths of the beams and the piezoelectric layer; $\mathrm{H}(y)$ is the Heaviside function to account for the fact that the piezoelectric layer does not cover the entire length of the beam. M_1 and M_2 are the masses of the magnets A, B and $w_b(t)$ represents the base displacement.

Considering the effect of electromechanical coupling, the potential energy of the whole system is

$$\begin{aligned} U &= U_1+U_2+W_e+U_m \\ &= \frac{1}{2}\int_0^{L_1} E_1I_1(w_1'')^2\mathrm{d}y-M_1gu_1(L_1,t) \\ &\quad -\int_0^{L_1} m_1gu_1\mathrm{d}y+\frac{1}{2}\int_0^{L_2} E_2I_2(u_2'')^2\mathrm{d}x \\ &\quad +\frac{E_2A_2}{2L_1}\left(\int_0^{L_1}(u_2')^2\mathrm{d}x\right)^2-\frac{F_0}{2}\int_0^{L_1}(u_2')^2\mathrm{d}x \\ &\quad -M_2gu_2(L_2/2,t)-\int_0^{L_2} m_2gu_2\mathrm{d}x \\ &\quad -\frac{1}{2}\int_0^{L_1}\gamma_c V w_1''\mathrm{d}y+\frac{1}{2}C_pV^2+U_m, \end{aligned} \tag{3}$$

where $(\cdot)$ and $(')$ indicate the differentiation with respect to time and length coordinate respectively; the flexural rigidity

of the piezoelectric beam is represented as

$$\begin{aligned} E_1 I_1 = & \frac{E_1 b {\delta_2}^3}{12}\Big[\mathrm{H}(y)-\mathrm{H}(y-L_1) \\ & -\mathrm{H}\Big(y-\frac{L_1-L_\mathrm{p}}{2}\Big)-\mathrm{H}\Big(y-\frac{L_1+L_\mathrm{p}}{2}\Big)\Big] \\ & +\frac{E_1 b({h_\mathrm{b}}^3-{h_\mathrm{a}}^3)+E_\mathrm{p} b({h_\mathrm{c}}^3-{h_\mathrm{b}}^3)}{3} \\ & \times\Big[\mathrm{H}(y)-\mathrm{H}(y-L_1)-\mathrm{H}\Big(y-\frac{L_1-L_\mathrm{p}}{2}\Big) \\ & -\mathrm{H}\Big(y-\frac{L_1+L_\mathrm{p}}{2}\Big)\Big], \end{aligned} \tag{4}$$

where E_1, E_2, and E_p denote the Young's modulus of the metal substrate and the piezoelectric layer, respectively; h_a, h_b, and h_c are the distance from the neutral axis to the bottom surface of the substrate, the distance between the neutral axis and the bottom surface of piezoelectric layer, and that between the neutral axis and the upper surface of the piezoelectric layer, respectively;[33] the flexural rigidity of the clamped beam is defined as $E_2 I_2 = E_2 b {\delta_2}^3/12$; $E_2 A_2$ is the extensional rigidity, where A_2 is the cross-sectional area of the clamped beam; F_0 represents the static axial force; and γ_c is the electromechanical coupling term, which can be given by

$$\begin{aligned} \gamma_\mathrm{c} = & \frac{E_1 d_{31} b L_\mathrm{p}({h_\mathrm{c}}^2-{h_\mathrm{b}}^2)}{\delta_1} \\ & \times\Big[\mathrm{H}\Big(y-\frac{L_1-L_\mathrm{p}}{2}\Big)-\mathrm{H}\Big(y-\frac{L_1+L_\mathrm{p}}{2}\Big)\Big], \end{aligned}$$

where d_{31} is the piezoelectric coupling coefficient; $C_\mathrm{P} = e_{33} b L_\mathrm{p}/\delta_\mathrm{p}$ is the capacitance of the piezoelectric material, where e_{33} is the permittivity at constant strain; $V(t)$ represents the voltage across the piezoelectric layer; U_m refers to the potential energy induced by magnetic forces.

The virtual works done by non-conservative forces are

$$\delta W = -c_1\int_0^{L_1}\dot{w}_1\delta w_1 \mathrm{d}y - c_2\int_0^{L_2}\dot{u}_2\delta u_2 \mathrm{d}x + Q(t), \tag{5}$$

where c_1 and c_2 are the damping coefficients introduced to approximate the energy loss from the viscous damping; $Q(t)$ is the electric charge of piezoelectric layer, and the time rate of change of it is the electric current passing through the resistive load R, i.e., $\dot{Q} = V/R$.

For the cantilever and clamped beams, their magnets' masses and positions are likely to induce the first modes of the beams; i.e., for vibrations of the two beams the first modes will be the dominant. Let ψ_1 and ψ_2 represent the first modes of the cantilever and clamped beams, respectively. Then, the displacement of the cantilever beam at y can be expressed as

$$w_1(y,t) = p(t)\psi_1(y), \tag{6}$$

and that of the clamped beam at x can be expressed as

$$u_2(x,t) = q(t)\psi_2(x), \tag{7}$$

where $p(t)$ and $q(t)$ denote the generalized temporal coordinates; ψ_1 and ψ_2 are the normalized mode shape functions of the two beams, respectively.

Considering the boundary conditions, $\psi_1(y)$ and $\psi_2(x)$ should take the following forms:[10,32]

$$\begin{aligned} \psi_1(y) &= 1-\cos\Big(\frac{\pi y}{2L_1}\Big), \\ \psi_2(x) &= (1-\cos(2\pi x/L_2))/2, \end{aligned} \tag{8}$$

the rotate angle θ at the free end of the cantilever beam can be approximated by

$$\theta = \arcsin({w_1}'(L,t)), \tag{9}$$

and the displacement perpendicular to $w_1(t)$ is

$$u_1 = \frac{1}{2}\int_0^y ({w'}_1(y,t))^2 \mathrm{d}y. \tag{10}$$

As shown in Fig. 2, in the process of calculating magnetic forces, the permanent magnets in the structure can be considered as point dipoles. In this figure, the red circles denote the unstable equilibrium positions. By their geometrical positions, the vector directed from the middle magnet (B) to the tip magnet (A) is denoted by $\boldsymbol{r}_\mathrm{BA}$ and can be expressed as

$$\boldsymbol{r}_\mathrm{BA} = p\hat{\boldsymbol{e}}_x - (d+u_1+q)\hat{\boldsymbol{e}}_y, \tag{11}$$

where $\hat{\boldsymbol{e}}_x$ and $\hat{\boldsymbol{e}}_y$ denote the unit vectors parallel and perpendicular to x axis. The magnetic moment vector $\boldsymbol{\mu}$ is dependent on the volume of magnet and is given in Ref. [14]

$$\boldsymbol{\mu} = \boldsymbol{M} V_\mathrm{m}, \tag{12}$$

where $\boldsymbol{M}$ represents the vector sum of all microscopic magnetic moments for ferromagnetic material, and V_m is the material volume. The magnetization vector $\boldsymbol{M}$ is related to magnet's residual flux density $\boldsymbol{B}_\mathrm{r}$, $\boldsymbol{M} = \boldsymbol{B}_\mathrm{r}/\mu_0$, where $\mu_0 = 4\pi\times10^{-7}$ H/m is the magnetic permeability constant.

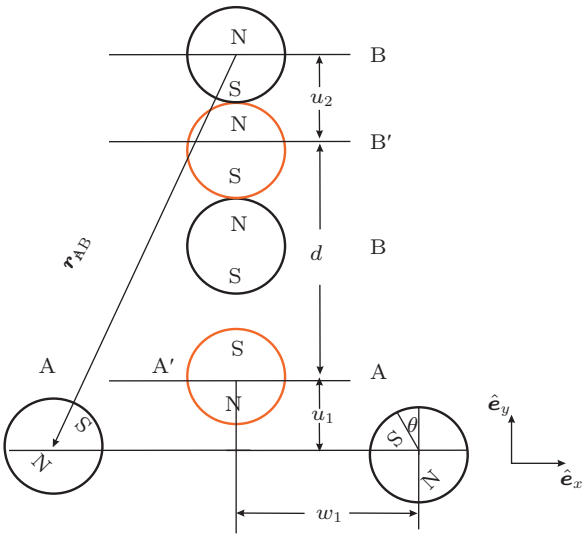


Fig. 2. (color online) Geometric diagram of magnetic dipoles.

Based on orthogonal decomposition, the magnetic dipole moment vectors take the following forms:[19]

$$\begin{aligned}\boldsymbol{\mu}_{\mathrm{A}} &= \boldsymbol{M}_{\mathrm{A}} V_{\mathrm{mA}} \sin\theta \hat{\boldsymbol{e}}_x + \boldsymbol{M}_{\mathrm{A}} V_{\mathrm{mA}} \cos\theta \hat{\boldsymbol{e}}_y,\\ \boldsymbol{\mu}_{\mathrm{B}} &= -\boldsymbol{M}_{\mathrm{B}} V_{\mathrm{mB}} \hat{\boldsymbol{e}}_y. \end{aligned} \tag{13}$$

The magnetic field of dipole B acting on dipole A is given by

$$\boldsymbol{B}_{\mathrm{BA}} = \frac{\mu_0}{4\pi} \nabla \frac{\boldsymbol{\mu}_{\mathrm{A}} \boldsymbol{r}_{\mathrm{AB}}}{\|\boldsymbol{r}_{\mathrm{BA}}\|_2^3}, \tag{14}$$

where $\|\cdot\|_2$ and ∇ denote the L_2-norm and the vector gradient operator respectively.

Thus, the potential energy of magnetic field can be written as

$$\begin{aligned} U_{\mathrm{m}} &= -\boldsymbol{\mu}_{\mathrm{A}} \boldsymbol{B}_{\mathrm{BA}}\\ &= \frac{\mu_0}{4\pi}\left(\frac{\boldsymbol{\mu}_{\mathrm{A}}\cdot\boldsymbol{\mu}_{\mathrm{B}}}{\|\boldsymbol{r}_{\mathrm{BA}}\|_2^3} - \frac{3(\boldsymbol{\mu}_{\mathrm{A}}\cdot\boldsymbol{r}_{\mathrm{BA}})(\boldsymbol{\mu}_{\mathrm{B}}\cdot\boldsymbol{r}_{\mathrm{BA}})}{\|\boldsymbol{r}_{\mathrm{BA}}\|_2^5}\right). \end{aligned} \tag{15}$$

The equivalent magnetic force can be obtained by

$$f_{12}(p,q) = \frac{\partial U_{\mathrm{m}}}{\partial p}; \quad f_{21}(p,q) = \frac{\partial U_{\mathrm{m}}}{\partial q}. \tag{16}$$

From Lagrange equation, the dynamical governing equations of the proposed system can be derived as follows:

$$\begin{aligned} &N_1\ddot{p} + N_2(p\dot{p}^2 + p^2\ddot{p}) + f_{12} + N_3\dot{p}\\ &+ N_4 p + N_5 V - N_6\ddot{w}_{\mathrm{b}}(t) = 0,\\ &C_{\mathrm{P}}\dot{V} + \frac{V}{R} - N_5\dot{p} = 0,\\ &N_7\ddot{q} + N_8 q + N_9 q^3 + f_{21} + N_{10}\dot{q} + N_{11} = 0, \end{aligned} \tag{17}$$

where

$$\begin{aligned} N_1 &= \int_0^{L_1} m_1 {\psi_1}^2 \mathrm{d}x + M_1,\\ N_2 &= m_1 \int_0^{L_1} \left(\int_0^y {\psi_1}'^2 \mathrm{d}y\right)^2 \mathrm{d}y + M_1\left(\int_0^{L_1} {\psi_1}'^2 \mathrm{d}y\right)^2,\\ N_3 &= c_1 \int_0^{L_1} {\psi_1}^2 \mathrm{d}y,\\ N_4 &= E_1 I_1 \int_0^{L_1} \psi_1''^2 \mathrm{d}y - M_1 g \int_0^{L_1} \psi_1'^2 \mathrm{d}y\\ &\quad - \int_0^{L_1} m_1 g \int_0^y \psi_1'^2 \mathrm{d}y\mathrm{d}y,\\ N_5 &= \int_0^{L_1} \gamma_{\mathrm{c}} {\psi_1}'' \mathrm{d}y, \quad N_6 = \int_0^{L_1} m_1 \psi_1 \mathrm{d}x + M_1,\\ N_7 &= \int_0^{L_2} m_2 {\psi_2}^2 \mathrm{d}x + M_2,\\ N_8 &= E_2 I_2 \int_0^{L_2} \psi_2''^2 \mathrm{d}x - F_0 \int_0^{L} \psi_2'^2 \mathrm{d}x,\\ N_9 &= \frac{E_2 A_2}{2L_2}\left(\int_0^{L_2} \psi_1'^2 \mathrm{d}x\right)^2,\\ N_{10} &= c_2 \int_0^{L} {\psi_2}^2 \mathrm{d}x, \quad N_{11} = M_2 \mathrm{g} + \int_0^{L_2} m_2 \psi_2 g \mathrm{d}x. \end{aligned}$$

For the BEH's governing equation, we can derive it by letting $u_2 = 0$; i.e., the clamped beam is considered as a rigid one. Thus the BEH's governing equation is

$$\begin{aligned} &N_1\ddot{p} + N_2(p\dot{p}^2 + p^2\ddot{p}) + f_{12}(p, q=0, t)\\ &+ N_3\dot{p} + N_4 p + N_5 V - N_6\ddot{w}_{\mathrm{b}}(t) = 0,\\ &C_{\mathrm{P}}\dot{V} + \frac{V}{R} - N_5\dot{p} = 0. \end{aligned} \tag{18}$$

The stability of the system is determined by the position of magnets A and B. Figure 3(a) shows how the shape of mechanical potential energy changes with the displacement of the magnets A and B. The mechanical potential energy is the sum of the elastic potential energy of the beams and the potential energy induced by magnetic forces. From Eqs. (3) and (15), it is known that the energy barrier is determined by the relative interval of the two magnets $|\boldsymbol{r}_{\mathrm{BA}}|$, which is influenced greatly by u_1, w_1, u_2, and d. As magnet A approaches magnet B, the interactive magnetic force will increase gradually such that the clamped beam is eventually forced to jump from the lower equilibrium point (−0.006 m) to the upper equilibrium point (0.006 m), which avoids the occurrence of strong interaction. Thus, the ABEH's barrier between the potential wells of potential energy will become lower due to the decrease in magnetic interaction (Fig. 3(b)).

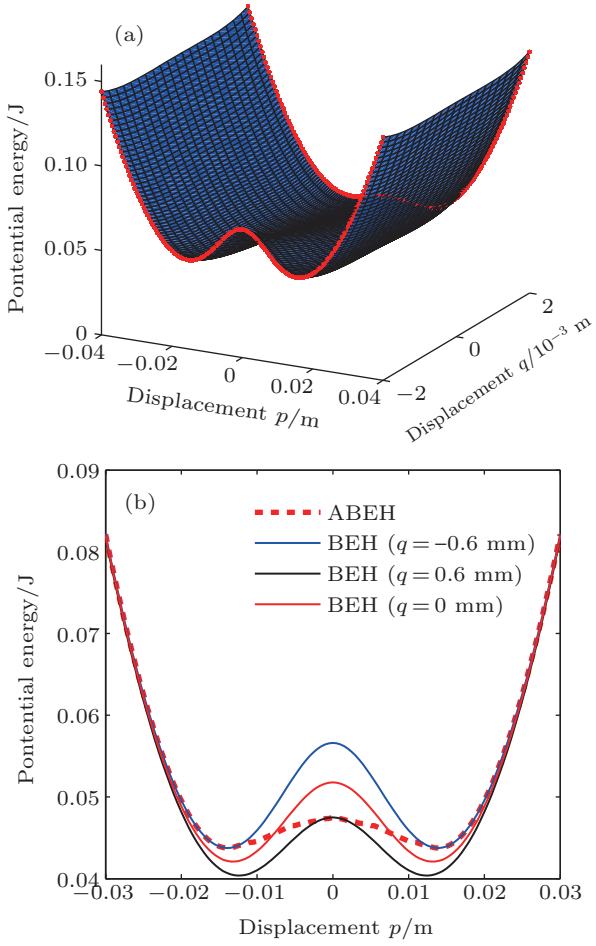


Fig. 3. (color online) Mechanical potential energy of the ABEH. (a) three dimensions; (b) two dimensions.

Given that the potential energy is known, the corresponding magnetic forces can be calculated by Eq. (16). Figure 4 shows the corresponding components of the magnetic force in x direction (f_{12}) and y direction (f_{21}). It is apparent that the magnetic force between magnets A and B is weak if the clamped beam moves in the positive direction ($q > 0$); i.e., it keeps away from the cantilever beam. In contrast, if the clamped beam moves in the negative direction ($q < 0$), i.e., it approaches the cantilever beam, then the magnetic force will become large. This is consistent with our knowledge regarding the magnetic repulsion force. Next we will focus on the comparison between the performances of the ABEH and BEH.

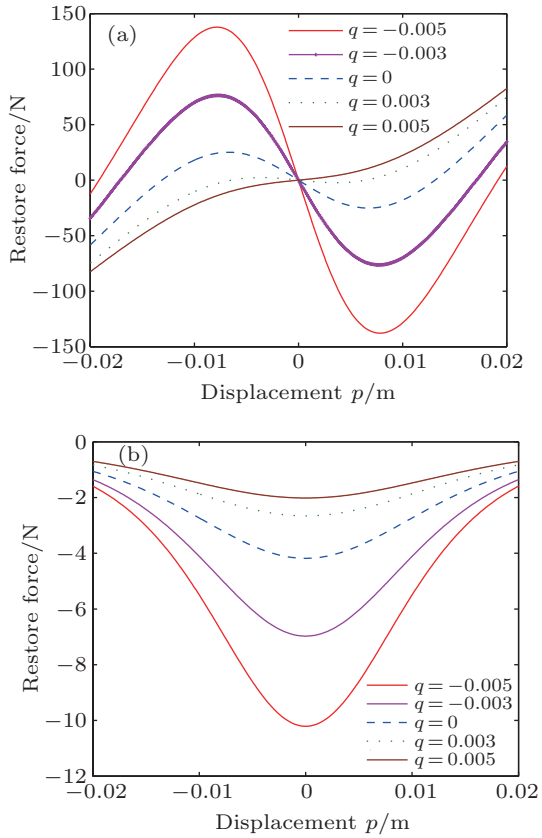


Fig. 4. (color online) Magnetic coupling forces. (a) x direction; (b) y direction.

3. Numerical simulation

3.1. The case of harmonic excitation

In this part, numerical simulations are carried out to investigate the dynamical response and electrical outputs of the two harvesters under frequency sweeping excitations. The base excitation is set as a harmonic motion governed by $\ddot{w}_b(t) = a_0 \sin(2\pi f t)$, where a_0 is the amplitude and f is the excitation frequency in unit of Hz. The range of the sweeping frequency is set 0–25 Hz, while the amplitudes of base excitations are designated as $a_0 = 2$ m/s^2 and $a_0 = 4$ m/s^2, respectively. The governing equations (Eqs. (17) and (18)) are solved by numerical method. The system parameters are set as Table 1, while the distance d is designated as 0.02 m. The simulation results are shown in Figs. 5 and 6, where the displacement refers to the tip deflection of the cantilever beam.

Table 1. Model parameters used for the numerical test.

Symbol, description	Value
length of cantilever beam, L_1	0.2 m
length of clamped beam, L_2	0.15 m
length of piezoelectric layer, L_p	0.02 m
width of beams and piezoelectric patch, b	0.02 m
thickness of cantilever beam, δ_1	0.0008 m
thickness of clamped beam, δ_2	0.0008 m
thickness of piezoelectric layer, δ_p	0.0008 m
Young's modulus of cantilever beam, E_1	210 Gpa
Young's modulus of clamped beam, E_2	69 Gpa
Young's modulus of piezoelectric layer, E_p	40 Gpa
density of cantilever beam, ρ_1	7800 kg/m^3
density of clamped beam, ρ_2	2700 kg/m^3
density of piezoelectric layer, ρ_p	7800 kg/m^3
static axial force, F_0	66.6 N
damping coefficient, c_1	0.1 N·s·m^{-1}
damping coefficient, c_2	0.1 N·s·m^{-1}
coupling coefficient, d_{31}	-280×10^{-12} C·N^{-1}
electrical permittivity, ε_{33}	3×10^{-8} F·N^{-1}
magnetization vector , M_A, M_B	0.995×10^{-6} A·m^{-1}
mass of magnet, M_1, M_2	0.012 kg
volume of magnet, V_A, V_B	$\pi \times 0.01^2 \times 0.005$ m^3
gravity acceleration constant, g	9.81 m·s^{-2}

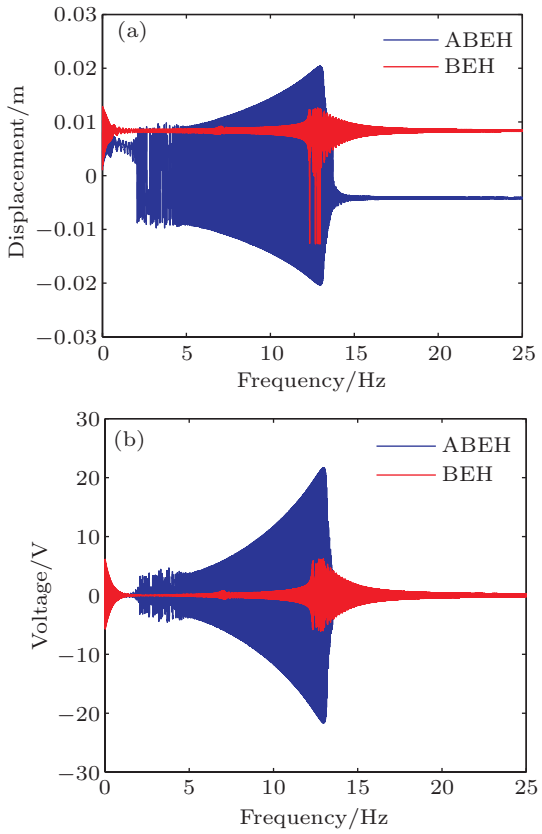


Fig. 5. (color online) Dynamical responses and output voltages as frequency sweeps ($a_0 = 2$ m/s^2). (a) Displacement; (b) voltage.

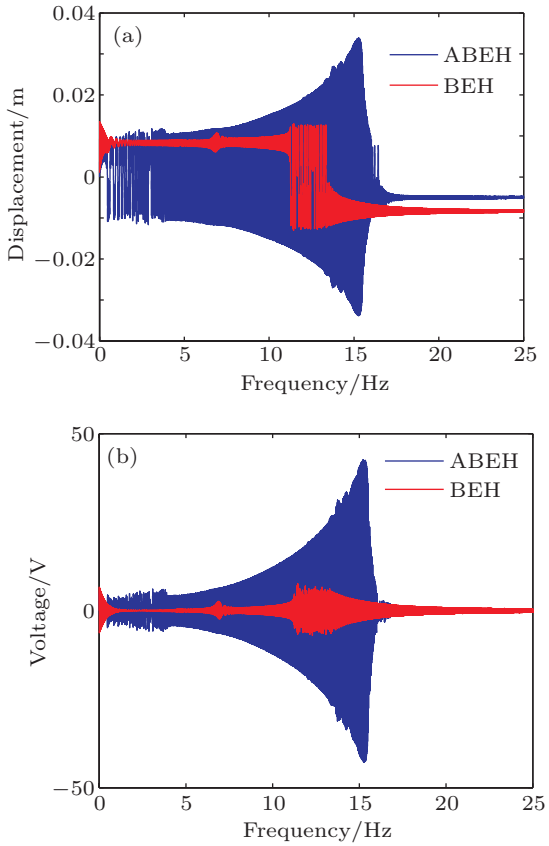


Fig. 6. (color online) Dynamical responses and output voltages as frequency sweeps ($a_0 = 4$ m/s^2). (a) Displacement; (b) voltage.

Comparisons between Figs. 5 and 6 suggest that the proposed energy harvester outperforms the traditional BEH in terms of both voltage amplitude and frequency bandwidth.

Figure 7 illustrates the variation of steady state RMS output voltage with the exciting frequency at $a_0 = 2$ m/s^2, from which we know that for $f < 9$ Hz the ABEH can generate higher RMS voltages than the BEH; and over the whole range of frequency, there appear some peaks of RMS voltage for both the BEH and ABEH. Specifically for the BEH, the peaks are at $f = 10.5$ Hz and 22.5 Hz, while for the ABEH, they are at $f = 9$ Hz and 16.5 Hz. For these frequencies, we calculate their responses respectively and depict the phase portraits and diagrams of the frequency spectrum (Figs. 8–11). First, at $f = 9$ Hz we can see that now the BEH's motion is restricted in a potential well, while the ABEH is undergoing an inter-well motion (Fig. 8). Then, at $f = 10.5$ Hz we find that the BEH enters to a chaotic state and exhibits irregularly jumping between the two equilibrium positions in the phase portrait, along with a large amplitude (Fig. 9(a)); from the corresponding frequency diagram we find that now the ABEH vibrates mainly at 3.5 Hz, 1/3 of the exciting frequency (Fig. 9(b)). Subsequently, at $f = 16.5$ Hz the ABEH undergoes a large amplitude of inter-well motion, while the BEH returns to an intra-well motion (Fig. 10(a)); it should be noted that now nearly all ABEH's vibration energy is concentrated at 5.5 Hz (1/3 of exciting frequency), while the BEH still keeps a synchronous response (Fig. 10(b)). Thus, it turns out that the ABEH seems to have the ability to move the exciting energy to a low-frequency response through sub-harmonic vibration and produce a relatively large amplitude. Finally, at $f = 22.5$ Hz, compared to the ABEH, the BEH has a fairly large amplitude although it is still in an intra-well state (Fig. 11(a)). From the corresponding frequency diagram, we know that now the ABEH's response is synchronized with the exciting frequency, while the BEH undertakes a sub-harmonic vibration, which results in a large amplitude (Fig. 11(b)).

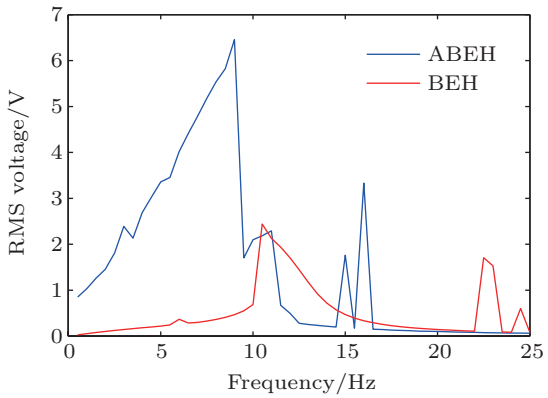


Fig. 7. (color online) Steady results of RMS voltage versus constant frequency excitation ($a_0 = 2$ m/s^2).

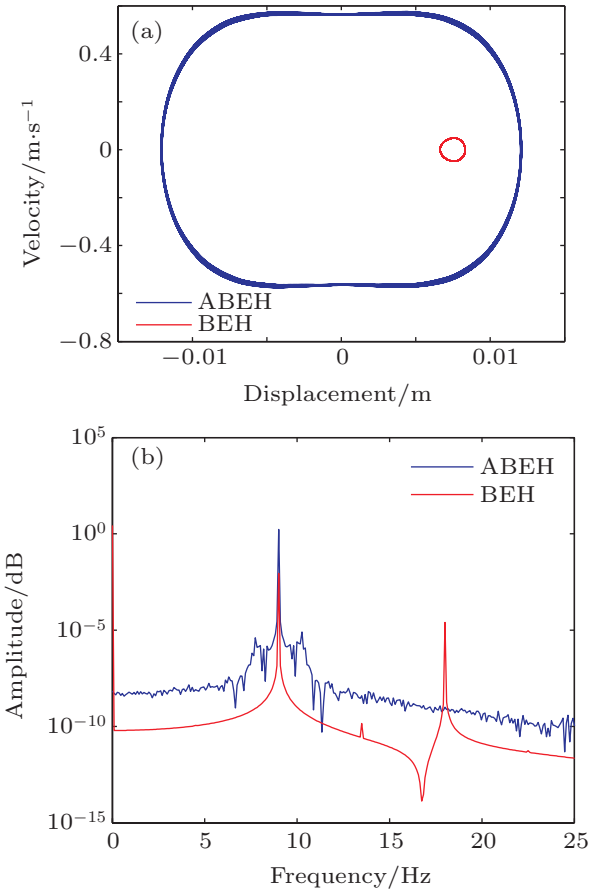


Fig. 8. (color online) (a) Phase portrait and (b) frequency spectrum at $f = 9$ Hz.

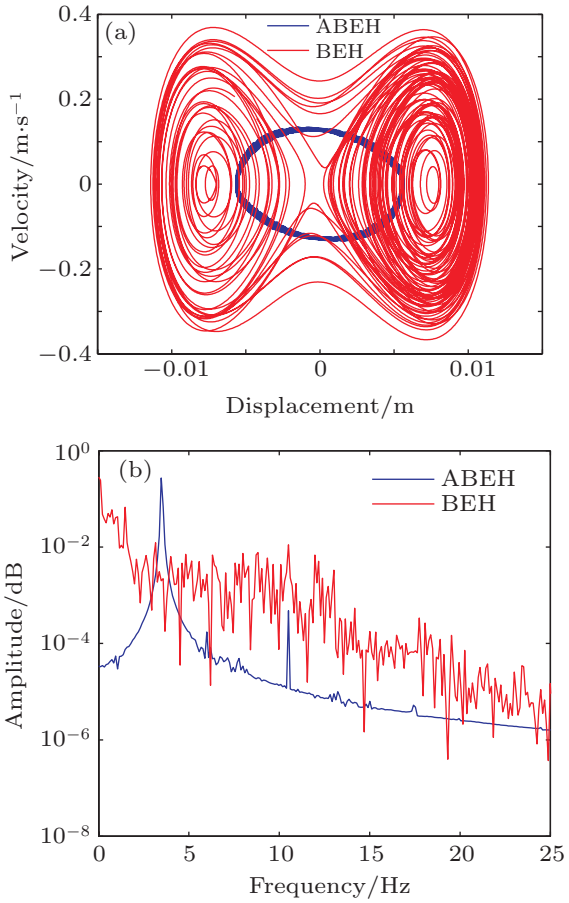


Fig. 9. (color online) (a) Phase portrait and (b) frequency spectrum (b) at $f = 10.5$ Hz.

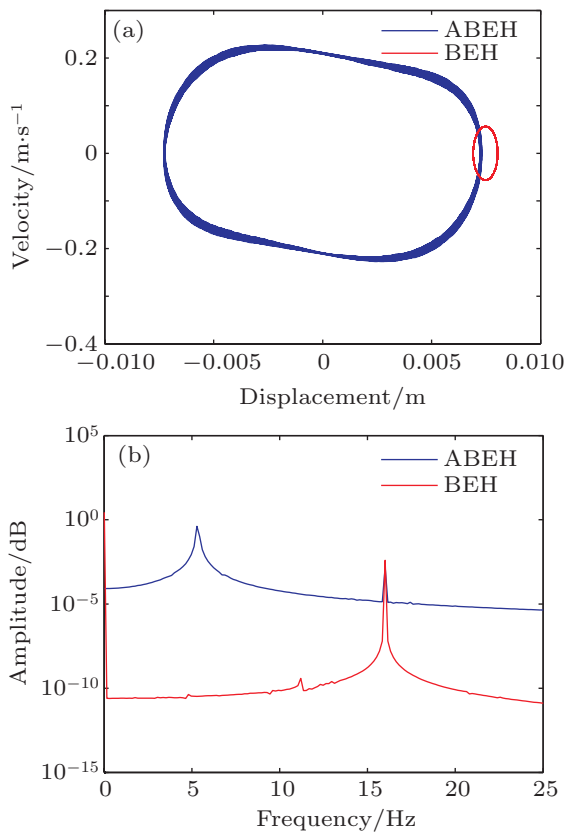


Fig. 10. (color online) (a) Phase portrait and (b) frequency spectrum at $f = 16.5$ Hz.

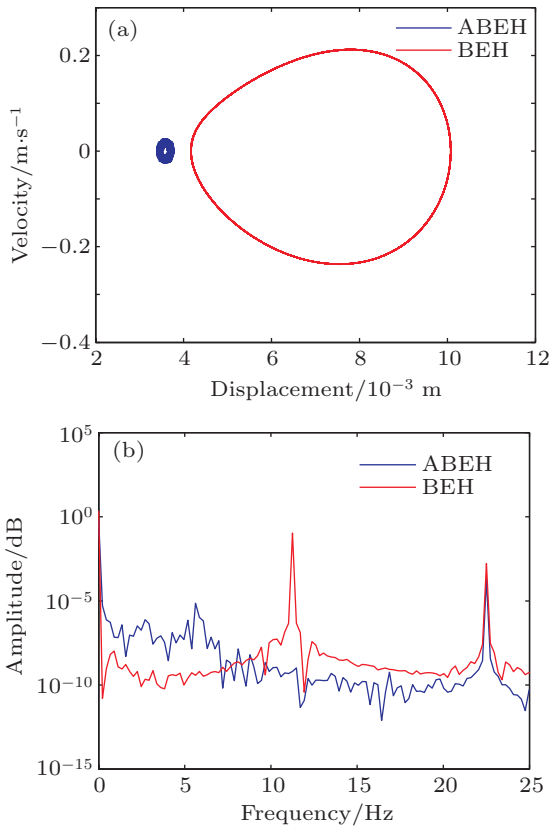


Fig. 11. (color online) (a) Phase portrait and (b) frequency spectrum at $f = 22.5$ Hz.

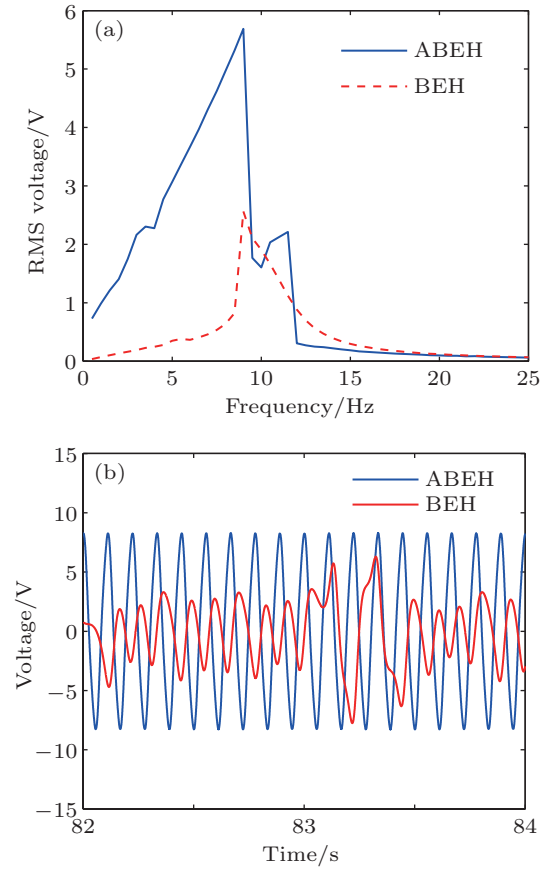


Fig. 12. (color online) (a) Frequency–voltage response and (b) the waveform of voltage at 9 Hz.

For the ABEH and BEH, we made some adjustments for system parameters to make their peak frequencies to reach identical. Figure 12 shows the resultant voltages at steady states for different frequency excitations, from which we learn that the peaks occur at $f = 9$ Hz for both systems. But we can see that at this frequency the ABEH's RMS voltage is considerably larger than that of the BEH (Fig. 12(a)). In terms of waveform (Fig. 12(b)), we know that at this frequency the ABEH has a larger amplitude than the BEH, especially the BEH's response is a chaotic one rather than a harmonic one. In addition, under the excitation level of $a_0 = 2$ m/s^2, the BEH's high energy range is $\Delta f = 1.5$ Hz, while that of the ABEH is $\Delta f = 2.75$ Hz. These findings also prove that the ABEH possesses a better harvesting performance.

3.2. The case of random excitation

To study the ABEH's harvesting ability under random excitations, we set the excitation as Gaussian white noise process $\ddot{w}_{\rm b}(t) = a(t)$, whose mean and correlation functions are given as follows:

$$\begin{aligned} &\langle a(t)\rangle = 0, \\ &\langle a(t)a(t+\Delta t)\rangle = 2\sigma_{\rm a}\delta(\Delta t), \end{aligned} \tag{19}$$

where $\langle\ \rangle$ denotes the expected value, and $\sigma_{\rm a}$ is the noise intensity.

The performance of the harvesting device can be evaluated in terms of RMS output voltage and efficiency of power conversion, defined by

$$\eta = \frac{P_{\rm e}}{P_{\rm m}}, \tag{20}$$

where $P_{\rm e}$ and $P_{\rm m}$ are the effective values of electrical and mechanical powers, respectively.

For an instantaneous power, its effective value is defined as

$$P = \sqrt{\frac{1}{t}\int_0^t (P^{\rm ins})^2\,{\rm d}t}, \tag{21}$$

where $P^{\rm ins}$ represents the instantaneous power at instant t. For the ABEH, its instantaneous electrical power harvested is defined as $P_{\rm e}^{\rm ins} = VI = V^2/R$, where I is the current, R the resistance; and its mechanical counterpart is defined as $P_{\rm m}^{\rm ins} = (N_6/N_1)a(t)\dot{p}$.[34]

The Euler–Maruyama method[35] and Monte–Carlo method are used in carrying out the stochastic simulation with parameters in Table 1. As the random excitation intensity $\sigma_{\rm a}$ increases, we calculate the corresponding dynamical responses and output voltages of the BEH and ABEH (Figs. 13 and 14). Figure 13 illustrates the signal to noise ratio (SNR = $\sigma_{\rm p}/\sigma_{\rm a}$,[24] where $\sigma_{\rm p}$ and $\sigma_{\rm a}$ represent the standard deviations of the response and the excitation, respectively) and the RMS voltage. In Fig. 13(a), it should be noted that the pronounced peak implies the occurrence of coherence resonance, in which the system can keep nearly regular jumps between the

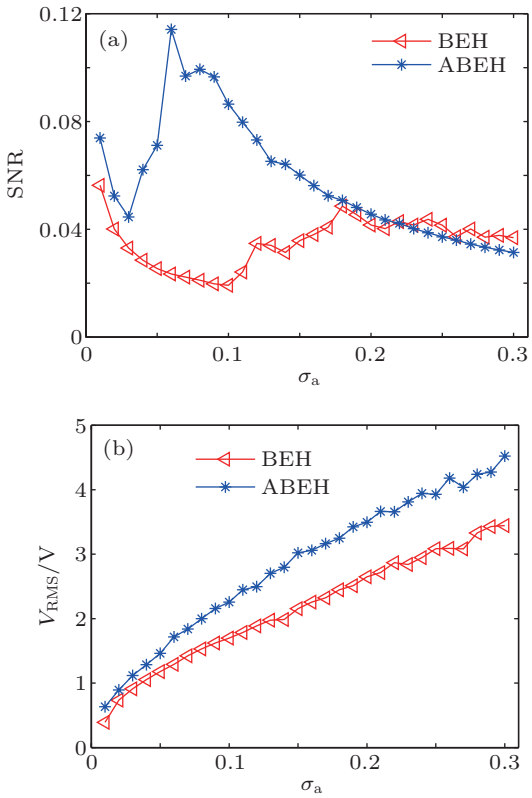


Fig. 13. (color online) (a) Signal-to-noise ratio and (b) RMS output voltage.

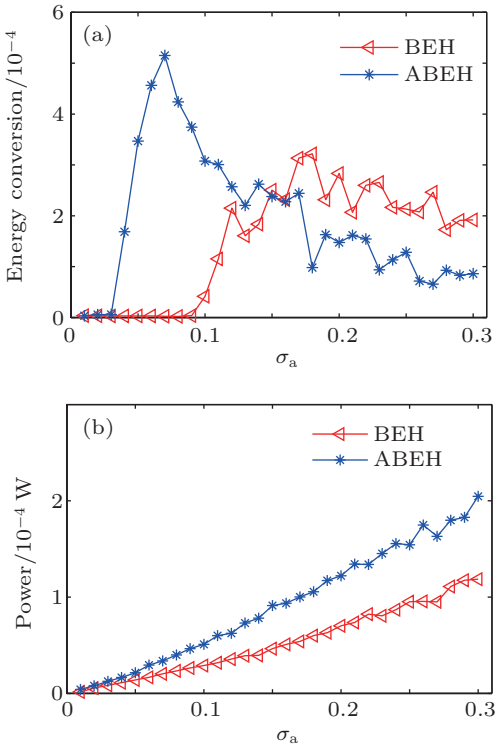


Fig. 14. (color online) (a) Energy conversion efficiency and (b) output power.

potential wells. The peak for the ABEH appears at $\sigma_a = 0.06$, while that for the BEH at $\sigma_a = 0.18$. This indicates that the ABEH can reach coherence resonance at a weaker excitation. Then, from Fig. 13(b), we know that the ABEH can generate a higher output voltage over the whole range of σ_a. Figure 14 illustrates the efficiency of energy conversion and the output power versus σ_a. This indicates that the ABEH is better than the BEH in the view of output power.

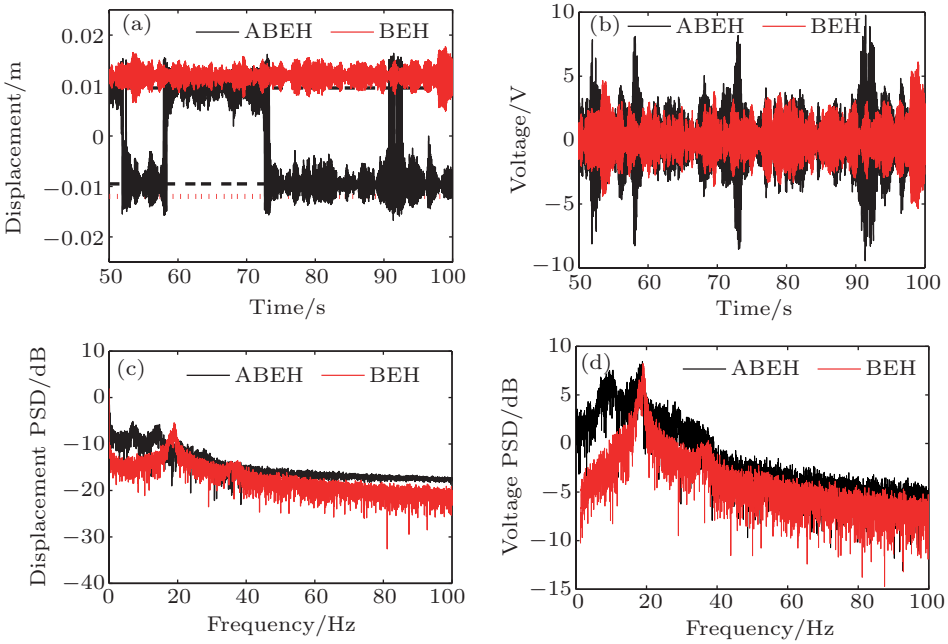


Fig. 15. (color online) Displacement and voltage responses at $\sigma_a = 0.07$. (a) Displacement, (b) voltage, (c) PSD of displacement, and (d) PSD of voltage.

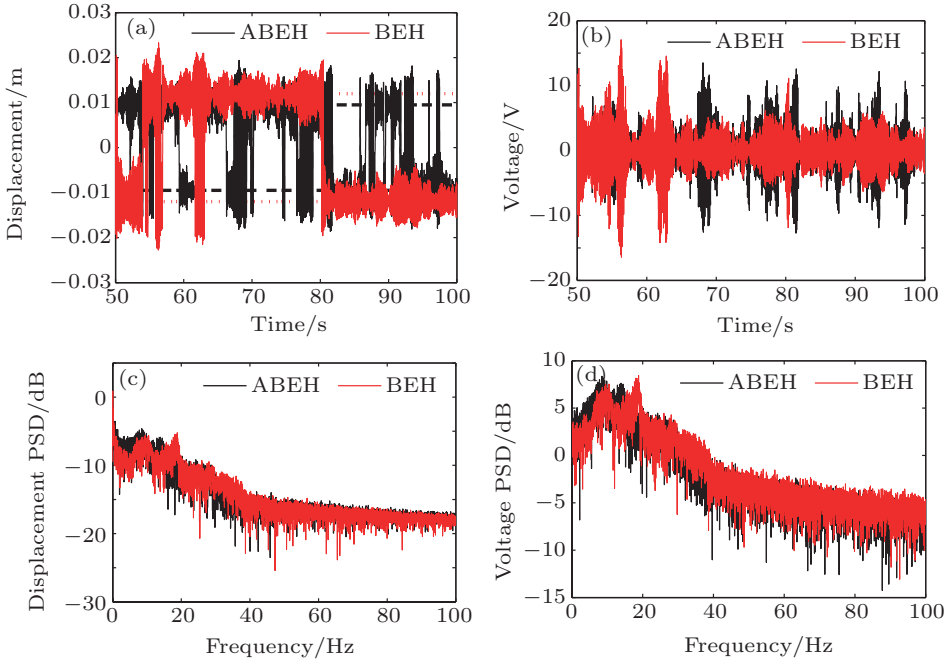


Fig. 16. (color online) Displacement and voltage responses at $\sigma_a = 0.3$. (a) Displacement, (b) voltage, (c) PSD of displacement, and (d) PSD of voltage.

Figures 15 and 16 show the time histories of the cantilever beam's tip displacements, the output voltages simultaneously generated by the piezoelectric material, the spectrum of displacement and the spectrum of voltage at $\sigma_a = 0.07$ and $\sigma_a = 0.3$, respectively. From the results, it can be seen that at $\sigma_a = 0.07$ the BEH's response is restricted in a single potential well, whereas jumping between the potential wells starts to occur in the ABEH (Fig. 15); and the highest output voltage of the ABEH can attain $V_{max} = 9.2$ V, while that of the BEH is only $V_{max} = 6.1$ V. As for the spectrum, figures 15(c) and

15(d) show PSDs of the displacement and voltage for ABEH and BEH. They prove the advantage of the ABEH. Then, as σ_a increases to 0.3, the BEH and ABEH both undergo jumping between potential wells. The BEH has a high potential barrier, which hinders frequently jumping between the potential wells. However, for the ABEH, its barrier is relatively low, which makes frequently jumping between the potential wells easy to occur, and thus it can give the higher output voltage. This can be clearly seen from the RMS output voltages for the two harvesters ($V_{\mathrm{RMS}}^{\mathrm{ABEH}} = 4.5$ V for the ABEH and $V_{\mathrm{RMS}}^{\mathrm{BEH}} = 3.5$ V for the BEH) (Fig. 13(b)). From the PSDs of the displacement and voltage (Figs. 16(c) and 16(d)), we can conclude that the ABEH can make an efficient electromechanical energy conversion under stochastic excitation.

4. Conclusion

This paper proposes an improved piezoelectric energy harvester having two bistable elastic beams coupling through their magnets. The coupling electromechanical equations are derived by the extended Hamilton's principle. Numerical simulations are carried out for harmonic and stochastic excitations. From the results, the following conclusions can be drawn.

1) Similar to the BEH, the presented ABEH has two stable equilibrium positions. But the original fixed magnet is replaced by a movable one mounted at the middle of a clamped beam. Thus, from the viewpoint of potential energy, the barrier height of ABEH becomes variable and is reduced. This design increases the possibility of jumping between the two potential wells.

2) The ABEH has a wider bandwidth of frequency for the occurrence of snap-through than the BEH. Thus, it can generate a higher output voltage than the BEH over nearly the whole range of sweeping frequency. The ABEH can transform the exciting energy to a low-frequency response by sub-harmonic effects, which brings about a large amplitude and output voltage. In particular, in the range of low frequency, its amplitude and output voltage exceed the BEH greatly.

3) Under random excitations, the ABEH can generate larger RMS output voltages and powers than the BEH over the whole range of excitation intensity σ_a. In particular, at weak excitations, it can realize snap-through and generate a considerably large maximum voltage. Therefore, it can be concluded that the ABEH is preferable in scavenging vibration energy.

References

[1] Priya S and Inman D J 2009 *Energy Harvesting Technologies* (New York: Springer) p. 135
[2] Erturk A and Inman D J 2011 *Piezoelectric Energy Harvesting* (New Jersey: John Wiley &Sons) p. 234
[3] Anton S R and Sodano H A 2007 *Smart Mater. Struct.* **16** R1
[4] Tang L, Yang Y and Soh C K 2012 *J. Intell. Mater. Syst. Struct.* **23** 1433
[5] Zhu D, Tudor M J and Beeby S P 2010 *Meas. Sci. Technol.* **21** 022001
[6] Daqaq M F 2012 *Nonlinear Dyn.* **69** 1063
[7] Jiang W A and Chen L Q 2010 *Mech. Res. Commun.* **53** 85
[8] Gafforelli G, Corigliano A, Xu R and Kim S G. 2014 *Appl. Phys. Lett.* **105** 203901
[9] Yang Z, Zhu Y and Zu J 2015 *Smart Mater. Struct.* **24** 025028
[10] Cottone F, Vocca H and Gammaitoni L 2008 *Phys. Rev. Lett.* **102** 080601
[11] Harne R L and Wang K W 2013 *Smart Mater. Struct.* **22** 023001
[12] Masana R and Daqaq M F 2012 *J. Appl. Phys.* **111** 044501
[13] Xu C D, Liang Z, Ren B, Di W N, Ruo H S, Wang D, Wang K L and Chen Z F 2013 *Appl. Phys. Lett.* **114** 114507
[14] Zhao S and Erturk A 2013 *Appl. Phys. Lett.* **102** 103902
[15] Jung J, Kim L P and Seok J 2015 *Int. J. Mech. Sci.* **92** 206
[16] Tékam G T O, Kwuimy C A K and Woafo P 2015 *Chaos* **25** 013112
[17] Kim P and Seok J 2014 *J. Sound Vib.* **333** 5525
[18] Zhou S, Cao J, Inman D J, Liu S S, Wang W and Lin J 2015 *Appl. Phys. Lett.* **106** 093901
[19] Stanton S C, McGehee C C and Mann B P 2010 *Physica D* **239** 640
[20] Erturk A and Inman D J 2011 *J. Sound Vib.* **330** 2339
[21] Moon F C and Holmes P J 1979 *J. Sound Vib.* **65** 275
[22] Wang G Q and Liao W H 2015 *Chin. Phys. Lett.* **32** 068503
[23] Zhou S, Cao J, Inman D J, Lin J Liu S S and Wang Z Z 2014 *Appl. Energ.* **133** 33
[24] Fan K Q, Xu C H, Wang W D and Fang Y 2014 *Chin. Phys. B* **23** 084501
[25] Litak G, Friswell M I and Adhikari S 2010 *Appl. Phys. Lett.* **96** 214103
[26] Li H T, Qin W Y, Deng W Z and Tian R L 2016 *EPJ Plus* **131** 60
[27] McInnes C R, Gorman D G and Cartmell M P 2008 *J. Sound Vib.* **318** 655
[28] Hu G, Ditzinger T, Ning C Z and Haken H 1993 *Phys. Rev. Lett.* **71** 807
[29] Lan C B, Qin W Y and Li H T 2013 *Acta Phys. Sin.* **22** 080503 (in Chinese)
[30] Cao J, Zhou S, Wang W and Lin J 2015 *Appl. Phys. Lett.* **106** 173903
[31] Hosseinloo A H and Turitsyn K 2015 *Phys. Rev. Appl.* **4** 064009
[32] Friswell M I, Ali S F, Bilgen O, Adhikari S, Lees A W and Litak G 2012 *J. Intel. Mat. Syst. Str.* **23** 1505
[33] Zhu Y, Zu J and Su W 2013 *Smart Mater. Struct.* **64** 045007
[34] De Paula A S, Inman D J and Savi M A 2015 *Mech. Syst. Signal. Pr.* **54–55** 405
[35] Zhao S and Erturk A 2013 *Smart Mater. Struct.* **22** 015002